Absolute Resonance Raman Intensity Analysis of Isopropyl Nitrate in the Condensed Phase

Ryan P. McLaughlin,† Bethany P. Nyholm, and Philip J. Reid*

Department of Chemistry, Box 351700, University of Washington, Seattle, Washington 98195

Received: May 14, 2003; In Final Form: August 18, 2003

The first resonance Raman spectra of isopropyl nitrate (IPN) are reported. Absolute resonance Raman scattering cross-sections for IPN dissolved in cyclohexane and acetonitrile are measured at excitation wavelengths spanning the strong $\pi-\pi^*$ absorption located at ~200 nm. Resonance enhancement is observed for seven vibrational coordinates, all involving the $-ONO_2$ chromophore, demonstrating that the photoinduced excited-state structural evolution is dominated by structural changes localized to the $-ONO_2$ group. The absorption and absolute resonance Raman cross-sections are modeled using the time-dependent formalism for absorption and Raman scattering. This analysis demonstrates that the photoinitiated excited-state structural-relaxation dynamics are multidimensional, and consistent with N−O bond cleavage. This observation is consistent with N−O bond dissociation being the dominant photodissociation pathway for larger (e.g., three or more carbon atoms) alkyl nitrates. Comparison of the results in cyclohexane and acetonitrile reveals that the excited-state structural evolution is solvent dependent. This observation suggests that the photoproduct formation dynamics of IPN are dependent on the environment in which the chemistry occurs.

Introduction

Trace gases are known to play a central role in the regulation of atmospheric ozone levels. Nitrogen oxides (NO, NO_2, and NO_3, collectively NO_x) are of particular interest because of their ability to both deplete and augment ambient ozone concentrations.[1−3] These species are commonly transported through the troposphere as relatively nonreactive reservoir compounds such as N_2O, peroxyacetyl nitrate (PAN), and N_2O_5. Alkyl nitrates ($RONO_2$, where R is an alkyl moiety) represent a large family of NO_x reservoir compounds.[4−7] Although a wide variety of alkyl nitrates (R = methyl, ethyl, isopropyl, etc.) have been detected in tropospheric environments, this entire class of compounds is thought to represent only a modest amount (~2%) of the total atmospheric NO_x budget.[5,8−14] However, alkyl nitrates have longer average lifetimes than other organic NO_x reservoir species, reflecting the relatively slow reaction rates between alkyl nitrates and OH radical, and their stability with respect to thermal decomposition. Therefore, though the abundance of alkyl nitrates in the atmosphere relative to other NO_x reservoir compounds is modest, their longer lifetimes allow them to obtain a wide distribution through the atmosphere.[2,7,10,15]

Reservoir compounds can release reactive constituents through thermal decomposition, OH radical scavenging, and/or photodissociation. Atmospheric models of alkyl nitrates have suggested that photodissociation becomes increasingly efficient relative to other loss mechanisms at higher altitudes.[1,2] As such, developing an understanding of alkyl nitrate photochemistry is an important component in predicting the impact of these compounds on NO_x levels in the upper atmosphere.[16,17] Several photodissociation pathways for alkyl nitrates have been proposed; however, only RO and NO_2 radical photoproducts are observed for gas-phase species having alkyl groups of three or more carbons, consistent with breakage of the weak O−N bond (~170 kJ/mol).[10,15,16] In contrast, RONO and O production has been observed for gaseous ethyl nitrate.[18] Current interest involves understanding the reasons behind this difference in photochemical reactivity, including variation in the photoinduced structural relaxation dynamics that dictate photoproduct formation dynamics.

To our knowledge, there has been no characterization of the condensed-phase photochemistry of alkyl nitrates. Heterogeneous processing of chlorine-containing reservoir species on polar stratospheric clouds has been shown to dramatically affect ozone levels.[3] Similarly, aerosol droplets and other particulate matter have also been shown to play an important role in tropospheric chemistry.[3] The multiphase nature of the atmosphere requires that a complete characterization of alkyl nitrate photochemistry include a description of the possible photodissociative pathways available to these compounds in condensed environments. The research outlined here was performed to address this issue.

This paper describes the first examination of the early-time photodissociation dynamics of isopropyl nitrate (IPN, presented in Figure 1) in the condensed phase using absolute resonance Raman intensity analysis (RRIA). Our studies were motivated by the large absorption cross-section of IPN and atmospheric abundance of this species relative to other alkyl nitrates.[19] In addition, vibrational assignments for IPN and isobutyl nitrate were recently reported such that an assignment of the Raman transitions to their corresponding normal coordinates is possible.[20] In these studies, absolute resonance Raman and absorption cross-sections are obtained and modeled to generate a mode-specific description of the optically prepared excited state. This information provides a description of the early-time reaction dynamics that occur following photoexcitation.[21−23] The results presented here demonstrate that the photodecomposition of IPN in solution is a multidimensional process with excited-state structural evolution dominated by evolution along several vibrational coordinates. The resonance Raman active normal coordinates are dominated by motion involving the $-ONO_2$

* To whom correspondence should be addressed. E-mail: preid@chem.washington.edu.

† Present address: Department of Chemistry, Seattle University, 900 Broadway, Seattle, WA 98122-4340.

10.1021/jp030620x CCC: $25.00
Published on Web 10/03/2003

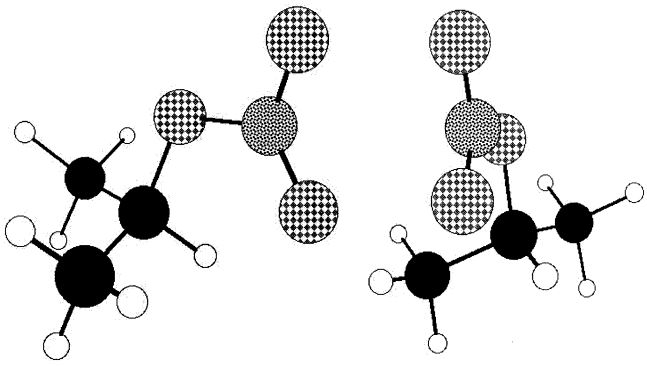

Figure 1. Two views of the optimized geometry for isopropyl nitrate calculated using B3LYP functionals with a 6-31G* basis set. The details of this calculation have been presented elsewhere.[20] Scheme: carbon (black), hydrogen (white), nitrogen (speckled), and oxygen (checkered).

chromophore, and in particular the N−O stretch. This observation demonstrates that the photoinduced excited-state structural evolution is consistent with N−O bond cleavage and structural relaxation of the $-ONO_2$ moiety. This picture of the excited-state reaction dynamics reflects the dominance of the N−O photochemical pathway for IPN and other alkyl nitrates for which the alkyl group has three or more carbon atoms. In addition, comparison of the results obtained in cyclohexane and acetonitrile reveals that the excited-state structural relaxation is solvent dependent. Specifically, excited-state displacement along the N−O stretch coordinate is enhanced in acetonitrile relative to cyclohexane such that evolution along this coordinate becomes a more prevalent component of the reaction coordinate in polar environments. This observation demonstrates that the photoproduct formation dynamics of IPN are dependent on the environment in which the chemistry occurs.

Experimental Section

Resonance Raman Spectra. Isopropyl nitrate was purchased (IPN, 96%, Aldrich) and used without further purification. The absolute resonance Raman scattering cross-sections of IPN were measured at 192.1, 208.8, 217.8, 228.7, 252.7, 282.4, and 532 nm using the hydrogen shifted and harmonic output of a Nd:YAG laser (Spectra-Physics GCL-170, 30 Hz). As will be shown below, the resonance Raman excitation profiles demonstrate minimal structure such that excitation at two wavelengths was judged to be sufficient to model the excited state of IPN in acetonitrile. Solution concentrations were adjusted at each excitation wavelength to provide comparable scattering intensity for both solute and solvent transitions. Sample solutions were pumped through a wire-guided jet at a sufficient rate to ensure that the illuminated sample volume was replenished between excitation events. A backscattering geometry (135°) was employed. The scattered light was collected using standard, UV-quality optics and delivered to a 0.75 m single-stage spectrograph (Acton Research Corp.) equipped with either a holographic 2400 or 3600 grooves/mm grating and a polarization scrambler placed at the spectrograph entrance. Scattering was detected with a liquid nitrogen cooled, back-illuminated CCD detector (Princeton Instruments). Spectra were corrected for the spectral sensitivity of the instrument using a calibrated D_2 emission lamp (Hellma). Data were not corrected for self-absorption; however, a comparison of solvent intensities with and without isopropyl nitrate showed intensities to be the same within 3%, demonstrating that self-absorption is extremely modest. Measurement of absolute scattering cross-sections also requires knowledge of depolarization ratios, defined as the intensity of light scattered with polarization perpendicular to that of the excitation light divided by the intensity of light scattered with polarization parallel to that of the excitation light.[24−27] Depolarization ratios were obtained by defining the incident beam polarization using a Glan Laser polarizer, and by passing the scattered light through a second polarizer placed immediately before the polarization scrambler. The intensity of radiation scattered parallel and perpendicular to the incident 218-nm radiation was measured by rotating the second polarizer to the appropriate orientation, and then collecting the scattered light as described above.

Absolute Scattering Cross-Sections. Absolute resonance Raman scattering cross-sections for IPN dissolved in cyclohexane were determined as follows. First, the scattering intensities of both the IPN transitions and the 802 cm^{-1} transition of cyclohexane were obtained by numerical integration of the peak areas. With the experimentally determined scattering intensities, the absolute Raman cross-sections were then calculated using

$$\frac{\sigma_{\mathrm{IPN}}}{\sigma_{\mathrm{C_6H_{12}}}} = \frac{I_{\mathrm{IPN}} C_{\mathrm{C_6H_{12}}}}{I_{\mathrm{C_6H_{12}}} C_{\mathrm{IPN}}} \frac{[(1+2\rho)/(1+\rho)]_{\mathrm{IPN}}}{[(1+2\rho)/(1+\rho)]_{\mathrm{C_6H_{12}}}} \quad (1)$$

In the above equation, c is the concentration, I is the integrated resonance Raman intensity, ρ is the depolarization ratio, and σ is the cross-section. Absolute scattering cross-sections for the 802 cm^{-1} transition of cyclohexane were obtained from the literature up to 218 nm, with extrapolation performed for shorter wavelength employing A-term fitting parameters described in the literature.[28,29]

Computational Modeling. Absorption and Raman cross-sections were modeled using the time-dependent formalism of Lee and Heller.[21−23,30,31] In this formalism, the Raman and absorption cross-sections are given by

$$\sigma_{\mathrm{R}}(E_{\mathrm{l}}) = \frac{8\pi E_{\mathrm{s}}^{\ 3} E_{\mathrm{l}} e^4 M_{\mathrm{eg}}^{\ 4}}{9\hbar^6 c^4} \int_{-\infty}^{\infty} \partial E_{00} H(E_{00}) \left| \int_0^{\infty} \langle f|i(t)\rangle e^{i(E_{\mathrm{l}}+E_{\mathrm{i}})t/\hbar} D(t)\, dt \right|^2 \quad (2)$$

$$\sigma_{\mathrm{A}}(E_{\mathrm{l}}) = \frac{4\pi e^2 E_{\mathrm{l}} M_{\mathrm{eg}}^{\ 2}}{6\hbar^2 cn} \int_{-\infty}^{\infty} \partial E_{00} H(E_{00}) \int_{-\infty}^{\infty} \langle i|i(t)\rangle e^{i(E_{\mathrm{l}}+E_{\mathrm{i}})t/\hbar} D(t)\, dt \quad (3)$$

where M_{eg} is the transition moment for the electronic transition of interest, E_{00} is the difference in energy between the ground and excited electronic states, E_{l} is the energy of the incident radiation, E_{s} is the energy of the scattered light, and E_{i} is the energy of the initial vibrational state. $D(t)$ is the homogeneous line width, which is composed of both pure dephasing and population decay. A Gaussian functional form for the homogeneous line width best reproduced the red edge of the absorption spectrum, and was therefore employed in this study. In this limit, $D(t) = \exp(-\Gamma^2 t^2/\hbar^2)$, where Γ is the homogeneous line width. The $H(E_{00})$ term in eqs 2 and 3 represents the inhomogeneous broadening corresponding to the distribution of E_{00} energies created by different solvent environments that are static on the time scale of Raman scattering, with this distribution modeled as Gaussian. Although inhomogeneous broadening was investigated, the breadth of the absorption spectrum and the absolute resonance Raman cross-sections could be reproduced using only homogeneous broadening; therefore, inhomogeneous broadening was not included in the final results presented here. The $\langle f|i(t)\rangle$ term in eq 2 represents the overlap

of the final state of the scattering process with the initial state propagating under the influence of the excited-state Hamiltonian, where $\langle i|i(t)\rangle$ in eq 3 represents the overlap of the initial ground state with the propagating state. The "super simple" model for the excited-state potential surface was employed in which the ground- and excited-state surfaces along each coordinate are modeled by harmonic potential having equivalent frequencies.[32,33] As such, the vibrational degrees of freedom are separable such that the multidimensional overlaps become the product of one-dimensional overlaps along each degree of freedom:

$$\langle i|i(t)\rangle = \prod_{k=1}^{3N-6} \langle i_k|i_k(t)\rangle \tag{4}$$

$$\langle f|i(t)\rangle = \langle f_1|i_1(t)\rangle \prod_{k=2}^{3N-6} \langle i_k|i_k(t)\rangle \tag{5}$$

The analytic expressions of Mukamel were then used to calculate the time-dependent overlaps along a each coordinate.[34,35] The analysis presented here provides a description of the slope of the excited-state potential energy surface in the Franck−Condon region of the excited state. Although photoexcitation of IPN promotes molecular dissociation such that the excited-state surface is clearly dissociative along at least one coordinate, the magnitude of the homogeneous line width dictates that the resonance Raman intensities are only sensitive to this slope in the Franck−Condon region. As such, the harmonic excited-state potentials employed here are used to determine the initial structural evolution experienced by IPN and are not intended to represent the excited-state potential at regions beyond the Franck−Condon accessed region of the excited state. The interested reader is directed to the literature for further discussion of this point.[21]

Results

Electronic Absorption Spectra. The electronic absorption spectrum of isopropyl nitrate (IPN) dissolved in cyclohexane and acetonitrile are presented as the solid lines in Figure 2A,B, respectively. There are two absorption bands in this region, a strong π to π^* transition located near 190 nm and a much weaker n to π^* transition near 265 nm. These two bands have been observed in the gas phase, and the spectrum reported here represents the first such measurement for this compound in solution.[8,17] The absorption cross-section for the π to π^* isopropyl nitrate transition in cyclohexane obtained in this work was 0.23 ± 0.04 Å^2 at 192 nm compared to the vapor-phase value of 0.18 Å^2.[8] The absorption spectrum in cyclohexane is identical in shape to the vapor-phase spectrum.[8] However, there is a red shift of the absorption maximum of approximately 5 nm in cyclohexane relative to the gas phase. The n to π^* transition cross-section for the solvated isopropyl nitrate is 0.0017 ± 0.0004 Å^2, showing enhancement over the 0.00046 Å^2 value for gaseous isopropyl nitrate at this same wavelength.[8] However, the cross-section for this transition is significantly smaller than that of the π to π^* transition such that this state is ignored in the spectral modeling described below. In acetonitrile, the absorption maximum occurs at 198 nm, red-shifted relative to cyclohexane. In addition, the absorption cross-section is reduced with a maximum value of 0.14 ± 0.03 Å^2. As illustrated in Figure 2, the π to π^* transition is featureless, suggesting that rapid dissociation occurs following photoexcitation.

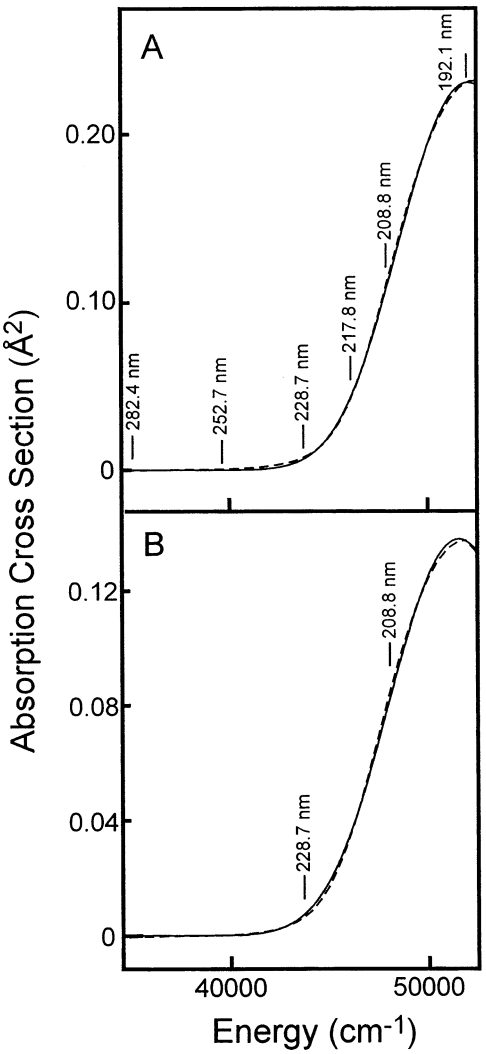

Figure 2. (A) Absorption spectra for IPN dissolved in cyclohexane (dashed line). The strong $\pi-\pi^*$ transition is evident. Best reproduction of the absorption spectrum using the time-dependent formalism is also shown (solid line). (B) Absorption spectra for IPN dissolved in acetonitrile (dashed line). Best reproduction of the absorption spectrum using the time-dependent formalism is also shown (solid line). The parameters employed in the calculations for both solvents are presented in Table 3. Excitation wavelengths employed in the resonance Raman studies are depicted.

Resonance Raman Intensity Analysis. Raman spectra of isopropyl nitrate were obtained with excitation at 192.1, 208.8, 228.7, 252.7, 282.4, and 532 nm in cyclohexane, and at 208.8 and 228.7 nm in acetonitrile. A subset of the spectra obtained in cyclohexane is presented in Figure 3. As shown in the figure, the spectrum of IPN simplifies dramatically as resonance with the $\pi-\pi^*$ transition is approached. With 208.8 nm excitation, the spectrum is dominated by transitions corresponding to seven vibrational coordinates, with these coordinates involving atomic motion localized predominantly to the $-ONO_2$ chromophore. Six of these modes are the NO_2 asymmetric (1626 cm^{-1}) and symmetric (1278 cm^{-1}) stretches, the N−O stretch (877 cm^{-1}), the NO_2 rock (850 cm^{-1}), the NO_2 scissor mode (705 cm^{-1}), and the CH wag (1345 cm^{-1}). A depiction of the internal coordinate contributions to these normal modes is presented in Figure 4. The seventh mode to demonstrate significant resonance enhancement is the NO_3 inversion mode. In the limit of C_s symmetry, this mode is non-totally symmetric with respect to reflection; therefore, fundamental intensity along this coordinate is not expected by symmetry. However, the overtone of this

TABLE 1: Measured Raman Cross-Sections for Isopropyl Nitrate in Cyclohexane

	192.1 nm[a]	208.8 nm	217.8 nm	228.7 nm	252.7 nm	282.4 nm
NO_2 scissor		1.04 ± 0.10[b]		0.09 ± 0.04		0.001 ± 0.001
NO_2 rock	4.98 ± 0.76	3.56 ± 0.39	0.76 ± 0.05	0.40 ± 0.04	0.07 ± 0.03	0.02 ± 0.01
NO str	5.00 ± 0.80	2.67 ± 0.33	0.66 ± 0.03	0.28 ± 0.08	0.02 ± 0.01	0.005 ± 0.001
NO_2 symm str	36.2 ± 3.9	21.4 ± 1.2	6.29 ± 0.20	2.01 ± 0.11	0.20 ± 0.07	0.03 ± 0.01
CH Wag	3.57 ± 0.20	1.91 ± 0.25	0.70 ± 0.20	0.20 ± 0.03	0.05 ± 0.01	0.01 ± 0.006
NO_3 inv overtone	5.10 ± 0.62	3.00 ± 0.34	1.14 ± 0.16	0.35 ± 0.02	0.022 ± 0.005	0.002 ± 0.001
NO_2 asymm str	12.8 ± 1.5	10.3 ± 0.2	4.32 ± 0.50	1.08 ± 0.10	0.10 ± 0.03	0.03 ± 0.01

[a] Cross-sections are $\times 10^{-9}$ Å^2. [b] Error represents one standard deviation from the mean of the number of measurements taken (≥ 3).

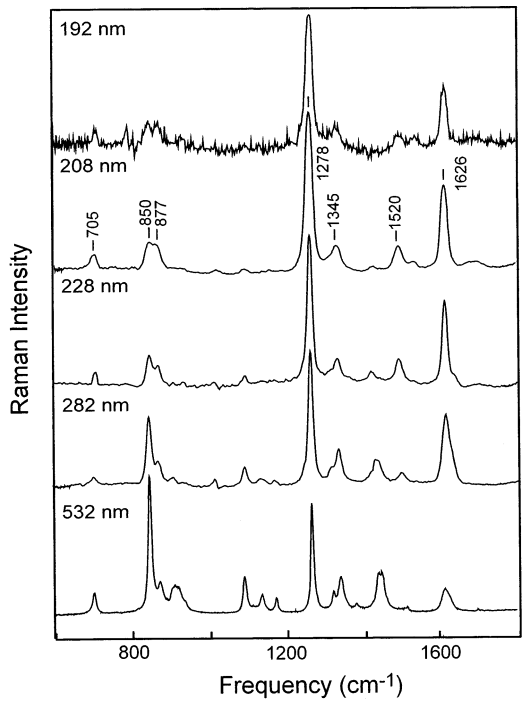

Figure 3. Raman spectra of isopropyl nitrate dissolved in cyclohexane obtained at five representative excitation wavelengths. The transitions that demonstrate resonance enhancement include fundamentals corresponding to the NO_2 scissor mode (705 cm^{-1}), the NO_2 rock (850 cm^{-1}), the N−O stretch (877 cm^{-1}), the NO_2 symmetric stretch (1278 cm^{-1}), the C−H wag (1345 cm^{-1}), and the NO_2 asymmetric stretch (1626 cm^{-1}). In addition to these transitions the overtone of the 760 cm^{-1} NO_3 inversion mode (1520 cm^{-1}) is also evident. Assignments correspond to those presented in the literature.[20] The weak transition at lower frequency next to the NO_2 asymmetric stretch fundamental is a combination of the NO_2 rock and the NO stretch. The weak mode located at approximately 1555 cm^{-1}, between the NO_3 inversion overtone and the NO_2 asymmetric stretch, is a combination band of the NO_2 scissor mode and the NO stretch.

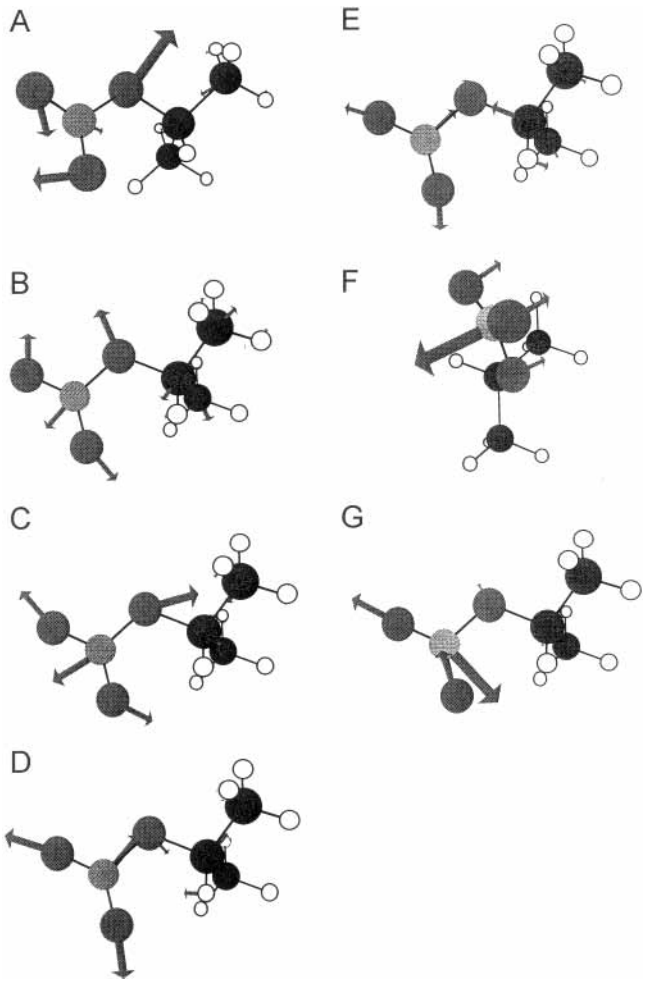

Figure 4. Depictions of the normal modes which demonstrate resonance Raman activity: (A) NO_2 scissoring, (B) NO_2 rock, (C) N−O stretch, (D) NO_2 symmetric stretch, (E) C−H wag, (F) NO_2 inversion, and (G) NO_2 asymmetric stretch. Vibrational modes are those calculated using B3LYP functionals with a 6-31G* basis set as described elsewhere.[20]

coordinate is observed at 1520 cm^{-1}, demonstrating that the curvature of the excited-state potential energy surface along this coordinate differs significantly from that of the ground state. Previous ab initio computational work and normal mode assignment studies by our group determined that the vibrational spectroscopy of IPN was consistent with a significant twist about the C−O bond and that the C_s-symmetry structure is approximately 2.6 kcal/mol higher in energy than this twisted structure.[20] This result is interesting in light of the absence of significant fundamental intensity for the NO_3 inversion mode implying that C_s symmetry is operative. The absolute scattering cross-sections for all of these transitions measured at the excitation wavelengths employed are presented in Tables 1 and 2 for cyclohexane and acetonitrile, respectively.

The π to π^* transition dominates the absorption spectrum of IPN such that when excitation resonant with this transition is employed, the observed intensities should be determined exclusively by this transition. If this is the case, the Raman-active transitions are expected to demonstrate a depolarization ratio of one-third. To test this assumption, depolarization ratios were measured at 218 nm and all seven major vibrational modes, as well as the overtone, exhibited ratios of one-third (within experimental error) with the exception of the asymmetric stretch transition (0.66 ± 0.03). Though it is clear (Figure 3) that there is a second vibrational transition located near the NO_2 asymmetric stretch, this transition demonstrates essentially no intensity at 218 nm and, therefore, should have little effect on the measured asymmetric stretch depolarization ratio. Although the origin of the depolarization ratio value of 0.66 is uncertain, the single state description was still deemed a reasonable approximation for this molecule and was used in the calculation of the absolute intensities.

TABLE 2: Measured Raman Cross-Sections for Isopropyl Nitrate in Acetonitrile

	208.8 nm[a]	228.7 nm
NO_2 scissor	0.3 ± 0.1[b]	0.03 ± 0.01[b]
NO_2 rock	1.0 ± 0.4	0.10 ± 0.03
NO str	1.3 ± 0.4	0.12 ± 0.05
NO_2 symm str	3.9 ± 0.7	0.57 ± 0.18
CH wag	0.7 ± 0.1	0.02 ± 0.01
NO_3 inv overtone	0.3 ± 0.1	0.02 ± 0.01
NO_2 asymm str	3.0 ± 0.6	0.52 ± 0.18

[a] Cross-sections are $\times 10^{-9}$ Å^2 [b] Error represents one standard deviation from the mean of the number of measurements taken (≥ 3).

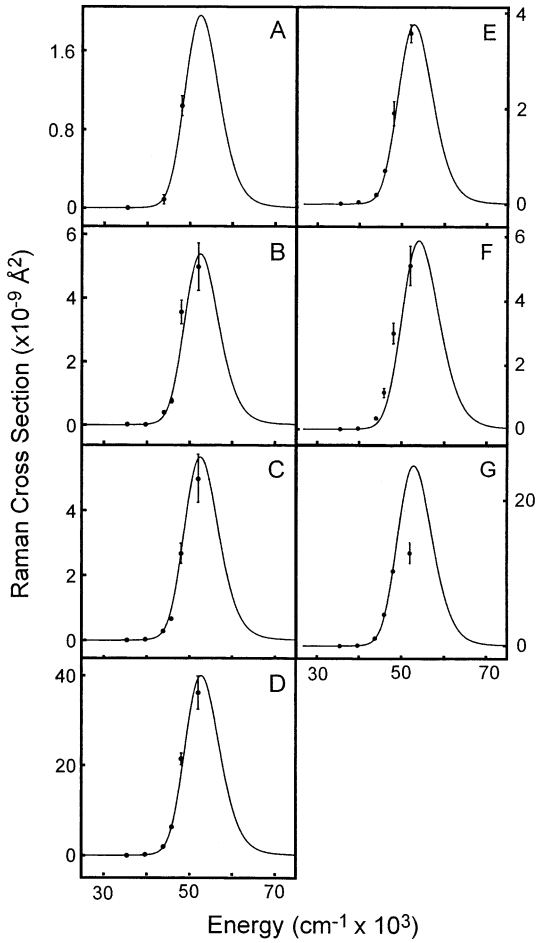

Figure 5. Experimental and calculated resonance Raman cross-sections for IPN in cyclohexane. Panels correspond to the following transitions: (A) NO_2 scissor fundamental, (B) NO_2 rock fundamental, (C) NO stretch fundamental, (D) NO_2 symmetric stretch fundamental, (E) CH wag fundamental, (F) NO_3 inversion first overtone, and (G) NO_2 asymmetric stretch fundamental. The points represent the experimental data with error bars defined as one standard deviation from the mean. Parameters employed in calculating the theoretical excitation profile (solid line) are provided in Table 3.

The absorption and Raman cross-sections were modeled using the time-dependent formalism as described above, and best reproduction of the experimental cross-sections obtained employing a Gaussian functional form for the homogeneous line width are shown in Figure 2 for the absorption spectrum. Figure 5 presents the REP's obtained in cyclohexane for the fundamental transitions involving the NO_2 scissor mode (A), the NO_2 rocking motion (B), the N−O stretch (C), the NO_2 symmetric stretch (D), the CH wag mode (E), the NO_3 inversion overtone (F), and the NO_2 asymmetric stretch (G). Figure 6 presents the corresponding information for IPN dissolved in acetonitrile. The absolute scattering cross-sections are well reproduced by the

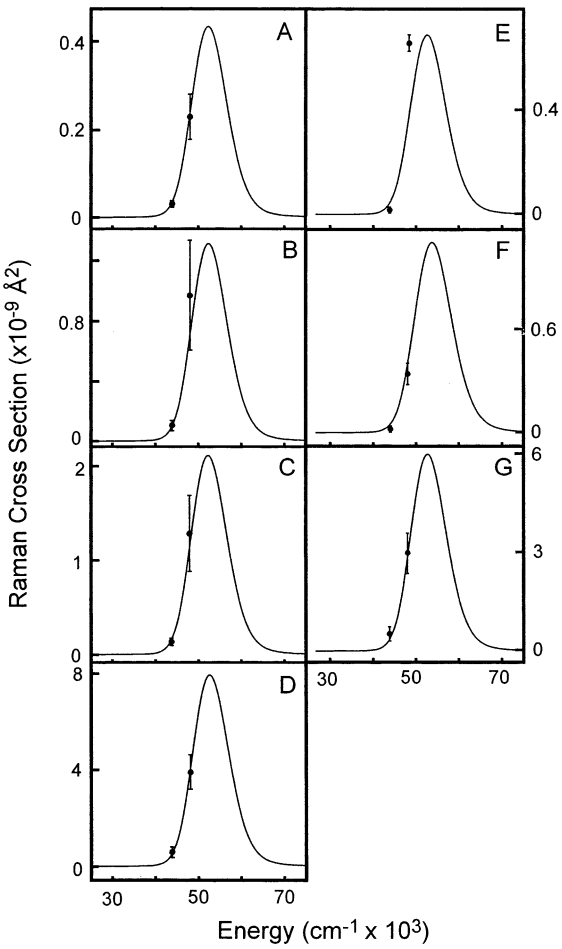

Figure 6. Experimental and calculated resonance Raman cross-sections for IPN in acetonitrile. Panels correspond to the following transitions: (A) NO_2 scissor fundamental, (B) NO_2 rock fundamental, (C) NO stretch fundamental, (D) NO_2 symmetric stretch fundamental, (E) CH wag fundamental, (F) NO_3 inversion first overtone, and (G) NO_2 asymmetric stretch fundamental. The points represent the experimental data with error bars defined as one standard deviation from the mean. Parameters employed in calculating the theoretical excitation profile (solid line) are provided in Table 3.

model for the excited-state potential energy surface, as are the absorption spectra (Figure 2).

As presented in Tables 1 and 2, the largest displacement occurs along the NO_2 symmetric stretch coordinate in both solvents, with the NO_2 rock, N−O stretch, and NO_2 asymmetric stretch coordinates also demonstrating significant displacement. This observation illustrates that the photoinitiated excited-state structural evolution is multidimensional, and not simply dominated by the N−O stretch. Reproduction of the absolute scattering intensities and breadth of the absorption spectrum required a Gaussian homogeneous line width of $\sim$1000 cm^{-1}, consistent with rapid evolution away from the Franck−Condon region of the optically prepared excited state followed by photodissociation. A more modest line width could be employed if the homogeneous line width was modeled as Lorentzian; however, recurrences in the absorption and Raman time correlators as well as a significant overestimation of the red-edge intensity of the absorption spectrum indicated that models employing a Lorentzian line width were inferior to the model presented here. The displacements listed in Table 3 were found to vary less than 10% relative to the model employing a Lorentzian homogeneous line width. In both cases, no inhomogeneous broadening was required, demonstrating that the broadening evident in the absorption spectrum is dominated by

TABLE 3: Excited-State Parameters for Isopropyl Nitrate in Cyclohexane and Acetonitrile[a]

vibrational mode	ν_g[b] (cm^{-1})	ν_e[b] (cm^{-1})	Δ(cxn)	σ_R(cxn exp)[c] ($\times 10^{-10}$ Å^2)	σ_R(cxn calc) ($\times 10^{-10}$ Å^2)	Δ(ace)	σ_R(ace exp) ($\times 10^{-10}$ Å^2)	σ_R(ace calc) ($\times 10^{-10}$ Å^2)
NO_2 scissor	705	705	0.95	0.9	1.0	0.90	0.3	0.3
NO_2 rock	850	850	1.31	4.0	2.8	1.30	1.0	1.0
NO str	877	877	1.30	2.8	2.9	1.60	1.2	1.5
NO_2 symm	1278	1278	2.40	20.1	18.2	2.15	5.7	5.6
CH wag	1345	1345	0.70	2.0	1.7	0.60	0.2	0.4
NO_3 inv overtone	760	1600	0.00	3.5	1.6	0.00	0.2	0.4
NO_2 asymm str	1626	1626	1.50	10.8	10.1	1.48	5.2	3.7

[a] Calculations in cyclohexane were performed with $\Gamma = 1200$ cm^{-1}, $M_{eg} = 0.77$ Å, $E_{00} = 44\,150$ cm^{-1}, and $n = 1.42$. Corresponding parameters for acetonitrile were $\Gamma = 1500$ cm^{-1}, $M_{eg} = 0.56$ Å, $E_{00} = 44\,250$ cm^{-1}, and $n = 1.344$. [b] ν_g refers to the ground-state frequency, and ν_e is the excited-state frequency. [c] Experimental and calculated Raman cross-sections correspond to 228.7 nm excitation.

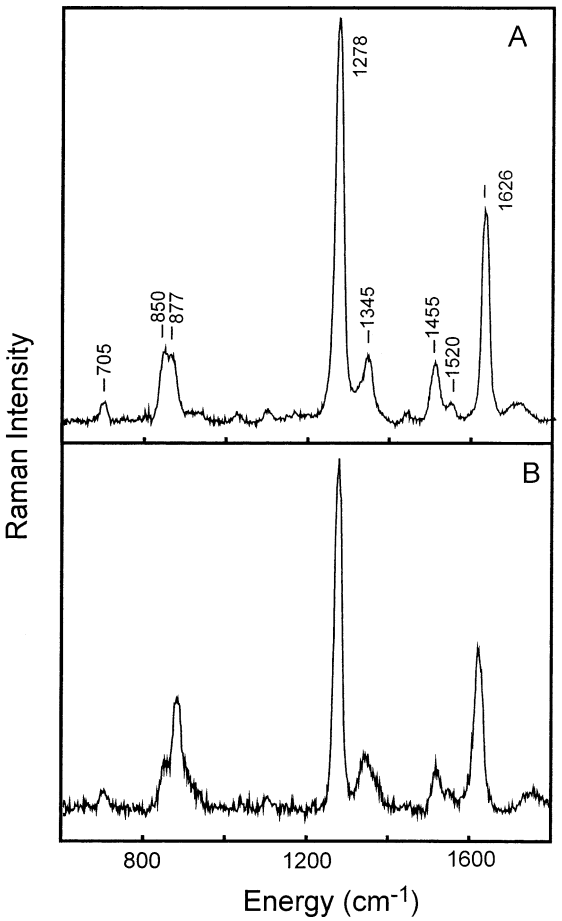

Figure 7. Resonance Raman spectra of IPN in cyclohexane (A) and in acetonitrile (B) obtained at 208.9 nm excitation. Note the increased relative intensity of the NO stretch fundamental transition (877 cm^{-1}) in acetonitrile relative to that of cyclohexane.

homogeneous processes, presumably reflecting rapid decay of the excited state. Rapid decay of the optically prepared excited state is also supported by the absence of detectable fluorescence from IPN.

Although the data obtained in cyclohexane and acetonitrile demonstrate many similarities, interesting differences are evident when the results from each solvent are compared. Figure 7 presents a comparison of the IPN resonance Raman spectra obtained using 208.8 nm excitation in cyclohexane and acetonitrile. A substantial difference in scattering intensity is observed for the transition at 877 cm^{-1} corresponding to the N−O stretch. Comparison of the excited-state displacements (Table 3) reveals that the increased intensity along this coordinate corresponds to increased excited-state displacement along this coordinate in acetonitrile relative to cyclohexane. The other coordinates demonstrate comparable displacements in both solvents. This result demonstrates that in polar solvents, the N−O stretch becomes a more prominent component of the photochemical reaction coordinate and indicates that the excited-state structural relaxation dynamics are dependent on the environment in which the photochemistry occurs.

Discussion

This primary gas-phase photodissociation pathway for larger (≥3 carbon atoms) alkyl nitrates is dissociation of the weak N−O bond to produce NO_2 and the corresponding alkoxy fragment. If similar photodissociation dynamics occur in the condensed phase, we would expect significant resonance enhancement for transitions involving the N−O stretch. As is illustrated in Figure 3, the fundamental transition of the N−O stretch demonstrates substantial resonance enhancement consistent with significant structural evolution along this coordinate. However, other modes demonstrate resonance enhancement, illustrating that photodissociation is a multidimensional process, and this observation suggests that other, minor photochemical channels may be operative in condensed environments. For example, breakage of one of the two N−O bonds would yield $(CH_3)_2CHNO_2$ and O, a pathway that has been observed for smaller alkyl nitrates in the gas phase.[18] This particular pathway is expected to be accompanied by motion along the asymmetric stretch coordinate of the nitrate group. The presence of resonance enhancement along this particular coordinate in IPN is consistent with, although certainly not conclusive of, dissociation of a terminal N−O bond.

With the normal mode analysis of IPN,[20] it is possible to interpret the dimensionless displacements determined in this analysis in terms of the extent of structural evolution that occurs upon photoexcitation.[36] Specifically, the internal-coordinate description of the normal-coordinates can be used to quantitatively describe molecular-geometry differences between the ground- and excited-state potential energy surface minima. This analysis is complicated by the fact that resonance Raman intensities are proportional to the square of the dimensionless displacement such that the sign of the displacement is not available. Therefore, assumptions must be made about the sign of the normal mode displacements in determining the extent of structural evolution. If we assume that the phase of the displacements is such that evolution along all coordinates results in one of the terminal N−O bonds becoming longer, then the following picture of photoinitiated structural evolution is derived. First, the central N−O bond undergoes dissociation in formation of the products such that an excited-state minimum is not expected along this coordinate. However, as mentioned above, the intensity of the N−O stretch indicates that substantial structural evolution occurs along this coordinate. The terminal N−O bonds are predicted to undergo elongation and compression of ~0.4 Å consistent with expected changes in bond order

accompanying formation of the NO_2 photoproduct. The prediction of one bond lengthening and the other shortening is a direct consequence of activity along the NO_2 asymmetric stretch. Finally, changes in C−O bond length are predicted to be exceedingly modest (∼0.01Å) consistent with minimal activity of the alkyl radical and NO_3 photoproduct channel. In summary, the resonance Raman intensities demonstrate that the structural evolution that occurs upon photoexcitation is entirely consistent with that expected for N−O dissociation resulting in the formation of $(CH_3)_2CHO$ and NO_2.

Comparison of the excited-state displacements obtained in cyclohexane and acetonitrile reveals that the excited-state reaction dynamics are solvent dependent. Specifically, the N−O stretch is found to make a larger contribution to the overall excited-state structural evolution in acetonitrile relative to cyclohexane. This observation suggests that the quantum yield for alkoxy radical production should be dependent on the environment in which the photochemistry occurs. Solvent dependence of the photoproduct quantum yield would demonstrate that the initial trajectory out of the Franck−Condon region of the optically prepared excited state is a defining aspect of the photochemistry, and that dissociation of the N−O bond is not simply due to the advent of intramolecular vibrational reorganization providing sufficient vibrational energy to promote bond dissociation. Studies are underway to characterize the later-time photochemistry of IPN, and to ascertain any solvent dependence in the photoproduct formation dynamics.

A second result of this study is that resonance Raman intensity was not observed for the overwhelming majority of transitions corresponding to the isopropyl moiety of IPN. This result demonstrates that significant structural rearrangement of the hydrocarbon portion of IPN does not occur upon photoexcitation and does not play a significant role in the dissociation process. In the normal mode analysis of IPN previously reported from our group, evidence was presented that the coupling between the nitrate moiety and the alkyl group in these compounds is weak.[20] The absence of significant resonance enhancement for transitions involving alkyl modes provides further evidence that IPN can be thought of as two separate groups. Weak coupling between these groups and the absence of excited-state structural evolution along the coordinates containing significant alkyl character suggests that breakage of the N−O bond should result in an alkoxy radical fragment that contains little excess vibrational energy. Time-resolved experiments capable of interrogating the distribution of photoproduct vibrational energy following photoexcitation should provide the evidence necessary to test this hypothesis.

Finally, it was previously reported that the ground-state structure of IPN was a nonsymmetric geometry (see Figure 1).[20] Though there is evidence that points to this assignment, it is based upon gas-phase computational results and a comparison of these calculations to the measured neat infrared spectrum. The presence of an overtone transition on resonance for the NO_3 inversion mode suggests that the structure of IPN in solution is close to C_s symmetry. Though the twisted structure of IPN was predicted to lie 2.6 kcal/mol lower in energy by our gas-phase density functional calculations, it is certainly possible that interactions with the solvent allow for the C_s structure to exist in solution, or that such interactions provide for only a modest twist of the C−O bond such that a proximate symmetry of C_s is applicable.

Conclusion

Characterization of the condensed-phase photodissociation dynamics of alkyl nitrates is important to understanding how these compounds are processed in the upper troposphere and lower stratosphere. As a step toward developing this understanding, we have reported the first resonance Raman spectra of isopropyl nitrate (IPN) in solution. Analysis of the absolute scattering cross-sections has shown that excited-state structural evolution occurs along several vibrational coordinates, demonstrating that the photodissociation of IPN is a multidimensional process involving coordinates localized on the $-ONO_2$ chromohore. Significant resonant enhancement is observed for transitions corresponding to the N−O stretch, consistent with dissociation of this bond dominating the gas-phase photochemistry. However, the multidimensional nature of the photodissociation process revealed by resonance Raman suggests that other photoproducts may be formed. Finally, the excited-state structural relaxation was found to be solvent dependent, suggesting that the photoproduct formation dynamics and quantum yields may vary as a function of environment.

Acknowledgment. The National Science Foundation is acknowledged for their support of this work (CHE-0091320). Acknowledgment is also made to the donors of the Petroleum Research Fund, administered by the American Chemical Society (P.J.R.). P.J.R. is an Alfred P. Sloan Fellow and is a Cottrell Scholar of the Research Corporation.

References and Notes

(1) Luke, W.; Dickerson, R. *Geo. Res. Lett.* **1988**, *15*, 1181.
(2) Luke, W.; Dickerson, R.; Nunnermacker, L. *J. Geophys. Res.* **1989**, *94*, 14905.
(3) Wayne, R. P. *Chemistry of Atmospheres*, 3rd ed.; Oxford University Press; Oxford, U.K., 2000.
(4) Atlas, E.; Pollock, W.; Greenberg, J.; Heidt, L.; Thomson, A. M. *J. Geophys. Res.* **1993**, *98*, 16933.
(5) Luxenhofer, O.; Ballschmiter, K. *Fresnius J. Anal. Chem.* **1994**, *350*, 395.
(6) Atlas, E. *Nature (London)* **1988**, *331*, 426.
(7) Talukdar, R. K.; Herndon, S. C.; Burkholder, J. B.; Roberts, J. M.; Ravishankara, A. R. *J. Chem. Soc., Faraday Trans.* **1997**, *93*, 2787.
(8) Turberg, J. M.; Giolando, D. M.; Tilt, C.; Soper, T.; Mason, D.; Davies, M.; Klingensmith, P.; Takacs, G. A. *J. Photchem. Photobiol.* **1990**, *51*, 281.
(9) Fischer, R. G.; Kastler, J.; Ballschmiter, K. *J. Geophys. Res.* **2000**, *105*, 14473.
(10) Clemitshaw, K.; Williams, J.; Rattigan, O.; Shallcross, D.; Law, K.; Cox, R. A. *J. Photochem. Photobiol., A: Chem.* **1997**, *102*, 117.
(11) Buhr, M. P.; Parish, D. D.; Norton, R. B.; Fehsenfeld, F. C.; Sievers, R. E.; Roberts, J. M. *J. Geophys. Res.* **1990**, *95*, 9809.
(12) Bottenheim, J. W.; Barrie, L. A.; Atlas, E. *J. Atmos. Chem.* **1993**, *17*, 15.
(13) Shepson, B.; Anlauf, K. G.; Bottenheim, J. W.; Wiebe, H. A.; Gao, N.; Muthuramu, K.; Mackay, G. I. *Atmos. Environ.* **1993**, *27A*, 749.
(14) Atlas, E.; Schauffer, S. M.; Merril, J. T.; Hahn, C. J.; Ridley, B. A.; Walega, J. G.; Greenberg, J.; Heidt, L.; Zimmerman, P. *J. Geophys. Res.* **1992**, *97*, 10311.
(15) Talukdar, R. K.; Herndon, S. C.; Burkholder, J. B.; Roberts, J. M.; Ravishankara, A. R. *J. Chem. Soc., Faraday Trans.* **1997**, *93*, 2797.
(16) Roberts, J. M. *Atmos. Environ., A* **1990**, *24*, 243.
(17) Zhu, L.; Kellis, D. *Chem. Phys. Lett.* **1997**, *278*, 41.
(18) Rebbert, R. E. *J. Phys. Chem.* **1963**, *67*, 1923.
(19) Atlas, E.; Schauffler, S. American Geophysical Union Fall Meeting, San Francisco, CA, 5−9 December, 1988.
(20) McLaughlin, R.; Bird, B.; Reid, P. J. *Spectrosc. Acta A* **2002**, *58*, 2571.
(21) Myers, A. B. *J. Raman Spectrosc*. **1997**, *28*, 389.
(22) Myers, A. B. *J. Opt. Soc. Am. B* **1990**, *7*, 1665.
(23) Myers, A. B.; Mathies, R. A. Resonance Raman Intensities: A Probe of Excited-State Structure and Dynamics. In *Biological Applications of Raman Spectrometry*; Spiro, T., Ed.; John Wiley & Sons: New York, 1987; Vol. 2, pp 1−58.
(24) Mortensen, O.; Hassing, S. Polarization and Interference Phenomena in Resonance Raman Scattering. In *Advances in Infrared and Raman Spectroscopy*; Clark, R., Hester, R., Eds.; Heyden: London, 1980; Vol. 6, p 1.
(25) Ziegler, L. *J. Chem. Phys.* **1986**, *84*, 6013.

(26) Ziegler, L.; Chung, Y.; Wang, C.; Zhang, Y. *J. Chem. Phys*. **1989**, *90*, 4125.

(27) Strommen, D. *J. Chem. Educ.* **1992**, *69*, 803.

(28) Li, B.; Myers, A. B. *J. Phys. Chem.* **1990**, *94*, 4051.

(29) Trulson, M. O.; Mathies, R. A. *J. Chem. Phys.* **1986**, *84*, 2069.

(30) Lee, S.-Y.; Heller, E. *J. Chem. Phys.* **1979**, *71*, 4777.

(31) Tannor, D.; Heller, E. *J. Chem. Phys*. **1982**, *77*, 202.

(32) Esposito, A. P.; Foster, C. E.; Beckman, R.; Reid, P. J. *J. Phys. Chem. A* **1997**, *101*, 5309.

(33) Foster, C. E.; Reid, P. J. *J. Phys Chem. A* **1998**, *102*, 3517.

(34) Sue, J.; Yan, Y.; Mukamel, S. *J. Chem. Phys.* **1986**, *85*, 462.

(35) Myers, A. B.;. Harris, R.; Mathies, R. A. *J. Chem. Phys.* **1983**, *79*, 603.

(36) The potential surface displacements (δ_α) are the displacement-weighted internal coordinate projections of the resonance Raman active normal modes, given by $\delta_\alpha = \Sigma_j \Delta_j a_{j\alpha}$, where $a_{j\alpha}$ are the internal coordinate projections for a given normal coordinate (j), Δ_j are the dimensionless displacements along a given normal coordinate as presented in Table 3, and Σ_j indicates that summation is taken over all normal coordinates.